A Novel Flexible Fault Eliminator with Active Disturbance Rejection and Soft Grid-Connection in Distribution Networks

Ze-Yin Zheng[1,2,*], Hao-Yu Qiu[1], Bin-Long Zhang[1], Mou-Fa Guo[1,2,**], Shuyue Lin[3], Wen-Qiang Cai[1]
[1]College of Electrical Engineering and Automation, Fuzhou University, Fuzhou 350108, China
[2]Engineering Research Center of Smart Distribution Grid Equipment, Fujian Province University, Fuzhou 350108, China
[3]Department of Engineering, University of Hull, Hull HU6 7RX, U.K.
[*]Corresponding authors: zhengzeyin@fzu.edu.cn
[**]Corresponding authors: gmf@fzu.edu.cn

Abstract: Among the possible fault types in the distribution networks, single-line-to-ground (SLG) fault has the highest probability. The SLG fault current and arc can easily cause personal injury and death. This study proposed a flexible fault eliminator (FFE) based on a cascaded H-bridge topology to limit the SLG fault current and extinguish fault arc in the medium voltage distribution networks. An active disturbance rejection controller for the FFE was designed to improve the current limiting performance of FFE in the presence of insulation parameter measurement errors and sampling errors from potential/current transformers. The controller with good robustness adapts to different ground fault resistances. In addition, a soft grid-connection control scheme based on bistable smooth switching was proposed to avoid the injected current impulse of FFE at the moment of grid connection. Simulation and experimental results showed that the fault current was limited to a small enough value and the fault arc was extinguished effectively. The output current and voltage of FFE at the time of grid connection were in a smooth transition, avoiding the impulse on the power grid system. The FFE can eliminate the SLG fault flexibly and stably.

Keywords: Flexible fault eliminator; active disturbance rejection control; soft grid connection; single-phase-to-ground fault arc suppression; distribution networks.

1. INTRODUCTION

The ground fault in distribution networks poses significant safety hazards and is unpredictable. Typically, single-line-to-ground (SLG) faults are the most common and can be caused by various issues [1], such as arrester breakdown, contact with foreign objects, line-to-crossbar discharge, insulator flashover, etc. In China, a distribution network with an isolated neutral point can continue to operate for up to two hours in the event of an SLG fault. However, it may lead to a temporary overvoltage during the operation of the SLG fault, which may exceed 2.3 p.u. in distribution networks. In certain situations, SLG faults would even evolve into cross-phase faults or multiple phase-to-ground faults [2]. In addition, long-time operations with SLG faults may increase the risk of life-threatening situations.

The installation of a Petersen coil at the neutral point is a widely used solution to reduce the SLG fault current and mitigate overvoltage and intermittent arcs [3]. The implementation of a resonant grounding system in distribution networks can significantly decrease SLG fault power by a factor of 10,000, thereby reducing the incidence of fires caused by tree branches in contact with overhead lines by over 90% [4]. However, the growing prevalence of cables in distribution networks can lead to an increase in the SLG fault current [5], resulting in a fast-growing demand to expand the capacity of the Petersen coil. Moreover, the current flowing through the Petersen coil cannot change abruptly. The residual overvoltage which exceeds 2 times the phase-to-ground voltage cannot be ignored [2]. The overturned Petersen coil designed to prevent resonance overvoltage may generate residual current, resulting in arc extinguishing failure. Furthermore, the ground fault current induced by the line-to-ground leakage resistances cannot be decreased by the Petersen coil.

Consequently, it is essential to install a reliable and flexible single-line-to-ground (SLG) fault current limiter. In [6]-[8], a flexible fault eliminator (FFE) based on a power electronic converter was connected to the neutral point in parallel with the Petersen coil to decrease the residual ground fault current. The Peterson coil compensates for most of the capacitive component of the SLG fault current and the FFE compensates for the residual capacitive and resistive components, achieving the full compensation of the ground fault current. However, the resonance overvoltage raised by the Peterson coil still cannot be avoided completely. With the development of power electronics technology, a high-capacity FFE based on a cascaded H-bridge (CHB) topology has been developed to replace the Petersen coil and limit the SLG fault current, so that the capacitive and resistive components of SLG fault current are compensated by the CHB converter, without the Peterson coil, thereby avoiding the resonant overvoltage [9]. However, due to the sub-accurate controller and modulation strategy, the FFE cannot track the reference current value accurately and promptly. Therefore, to minimize the error between reference and feedback signals in the discrete FFE control system, an improved distributed commutations modulation (IDCM) method that can adapt to the FFE operation characteristics was proposed, and successfully applied in the experimental prototype, with desired performance [10]. It is worth noting that the robustness of the FFE is crucial due to the variable ground fault resistance and changing operating conditions of distribution networks. The FFE should not only limit the ground fault current and prevent arc combustion but also ensure its stable operation without being affected by disturbances.

The proportional integral differential (PID) control method is widely used in industrial applications because of its simplicity and robustness [11]-[13]. However, the PID controller may not provide satisfactory tracking performance for fast-varying AC signals. Thus, an improved model predictive control method was employed to enhance the AC signal tracking performance [14]. Nevertheless, considering the non-linear characteristics of the SLG fault arc, the back-stepping control (BSC) can further improve the robustness of the FFE [9, 15]. However, measurement errors in insulation parameters and sampling errors from potential/current transformers may lead to poor fault current limiting performance and arc extinguishing failure. These cannot be addressed by the above control methods. Consequently, a disturbance rejection control technology needs to be explored to address these disturbances.

Active disturbance rejection control (ADRC) has been demonstrated as an effective alternative to PID control [16]. ADRC utilizes an error-driven control law inherited from PID control and a state observer obtained from modern control theory. It employs a simple differential equation as the transient profile generator and incorporates a noise-tolerant tracking differentiator and nonlinear feedback control to estimate and eliminate the impact of disturbances. Hence, the ADRC has emerged as a widely accepted technique in industrial applications. In addition, linear ADRC is a two-degree-of-freedom control that can be analyzed through the internal model control framework [17].

In [18], the ADRC was applied to the CHB rectifier to enhance its anti-interference performance as a superior alternative to the PID controller. In [19], the grid disturbance rejection controller and uncertainty rejection controller were designed to optimize the performance of the system under grid disturbances and parameter uncertainties. These controllers offer theoretical support to handle various disturbance scenarios, including SLG fault resistance variation, insulation parameter measurement deviations, and sampling errors from potential/current transformers. Moreover, ADRC has shown the potential to improve the damping performance of the grid-connected system, whose stability factor can be assessed by establishing the impedance models [20]. If the SLG fault resistance is considered part of the damping of grid-connected FFE, the variation of the SLG fault resistance can be regarded as a damping change. In this way, the disturbances caused by the arc variation during the SLG fault may be solved. In [21], the plant information and external disturbances were modeled as generalized disturbances and estimated using a linear extended state observer, which was incorporated into the linear state feedback control law for rapid rejection. The linear finite-dimensional controller can be implemented via the linear ADRC structure. In this paper, we design a linear ADRC system to resist generalized disturbances, including SLG fault resistance variation, insulation parameter measurement errors, and sampling errors from potential/current transformers.

Furthermore, it is important to consider the transient dynamics during the grid connection of FFE. At present, the research on the grid connection via power electronic converter focuses mainly on the synchronous operation with the power grid [22]-[25]. Especially in the case of power grid failure, the converter needs to keep synchronous operation with the power grid [26]. However, the power electronic converter can generate transient impulses during grid connection, which makes studying soft grid-connection technologies important but often overlooked. In [27], a flexible grid connection technique based on direct power control for unbalanced grids was proposed. In [28], a soft grid-connection technique was proposed that relied on zero-crossing detection, but this method is susceptible to harmonic disturbances. To address this issue, we propose a novel soft grid-connection control scheme based on bistable smooth switching and compare its effectiveness with that of the zero-crossing detection method. Our approach effectively reduces the current impulse of FFE on the power grid system during grid connection.

This paper was organized as follows: the principle of flexible fault elimination for distribution networks was introduced in Section II. The ADRC system design and soft grid-connection scheme for FFE were presented in Section III. The performance of FFE with ADRC and soft grid connection was verified by simulation in Section IV. The experimental results of the FFE industrial prototype were displayed in Section V. The conclusions were summarized in Section VI.

2. PRINCIPLE OF FLEXIBLE SINGLE-PHASE-TO-GROUND FAULT ARC SUPPRESSION

2.1 Distribution network with FFE

The distribution network with an FFE is shown in Fig. 1. G is the 110kV ideal power supply. The distribution network voltage is 10.5 kV converted from 110 kV via a transformer $\mathrm{T_{yd}}$. u_A, u_B, and u_C are the line-to-ground voltages, respectively. r_0A, r_0B, and r_0C are the line-to-ground leakage resistances, respectively. c_0A, c_0B, and c_0C are the line-to-ground capacitances, respectively. The line-to-ground currents are $i_{\mathrm{A}\Sigma}$, $i_{\mathrm{B}\Sigma}$, and $i_{\mathrm{C}\Sigma}$, respectively. It is assumed that the SLG fault occurs in phase A. The faulty phase voltage is $u_\mathrm{f} = u_\mathrm{A}$. The ground fault resistance is R_f, and the ground fault current is i_f. FFE consists of a CHB converter and filter inductor L_HN, and it is connected between the neutral-point N structured by the zigzag transformer $\mathrm{T_{zt}}$ and ground. The neutral-point voltage is u_0. The injected current and output voltage of FFE are i_HN and u_HN, respectively. The potential transformer (PT) is connected to the bus for sampling.

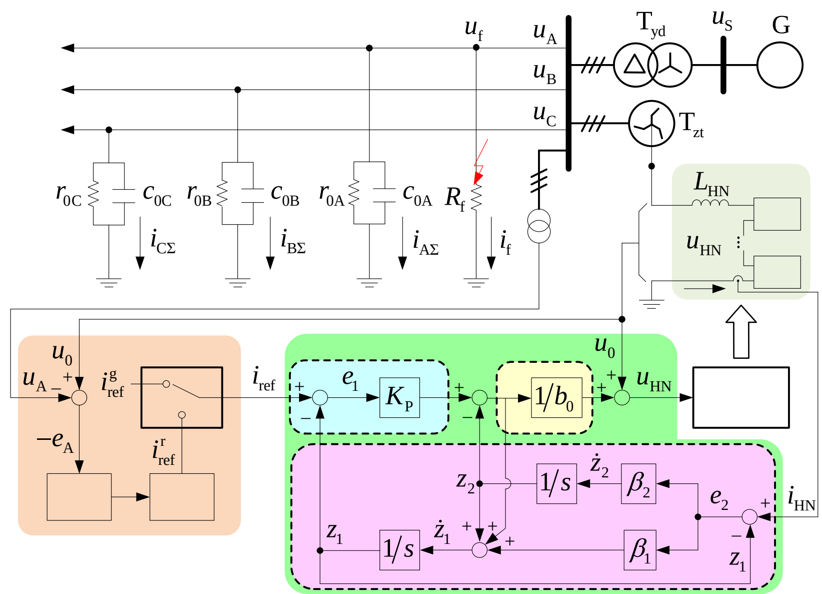

Fig. 1. Distribution network with FFE.

2.2 Principle of flexible fault elimination

Assuming that the three-phase power supply and the line-to-ground parameters are symmetrical. The line-to-ground leakage conductance and capacitance can be described as $G_0 = 1/R_0 = 1/r_\mathrm{0A} + 1/r_\mathrm{0B} + 1/r_\mathrm{0C}$ and $C_0 = c_\mathrm{0A} + c_\mathrm{0B} + c_\mathrm{0C}$, respectively. From Fig. 1, it can be presented that

$$i_\mathrm{HN} = \frac{u_\mathrm{A}}{r_\mathrm{0A}} + c_\mathrm{0A}\frac{\mathrm{d}u_\mathrm{A}}{\mathrm{d}t} + \frac{u_\mathrm{B}}{r_\mathrm{0B}} + c_\mathrm{0B}\frac{\mathrm{d}u_\mathrm{B}}{\mathrm{d}t} + \frac{u_\mathrm{C}}{r_\mathrm{0C}} + c_\mathrm{0C}\frac{\mathrm{d}u_\mathrm{C}}{\mathrm{d}t} + \frac{u_\mathrm{A}}{R_\mathrm{f}}. \tag{1}$$

The line-to-neutral voltages are denoted as e_A, e_B, and e_C, respectively. The line-to-ground voltage can be expressed by the line-to-neutral voltage and neutral-point voltage as

$$u_X = u_0 + e_X,\ X = \mathrm{A, B, C}. \tag{2}$$

Replacing (2) into (1), it can be rewritten as

$$\begin{aligned} i_{\mathrm{HN}} &= \frac{u_0}{R_0} + C_0\frac{\mathrm{d}u_0}{\mathrm{d}t} + \frac{u_{\mathrm{A}}}{R_{\mathrm{f}}} \\ &= \frac{u_{\mathrm{A}}}{R_0} + C_0\frac{\mathrm{d}u_{\mathrm{A}}}{\mathrm{d}t} - \left(\frac{e_{\mathrm{A}}}{R_0} + C_0\frac{\mathrm{d}e_{\mathrm{A}}}{\mathrm{d}t}\right) + \frac{u_{\mathrm{A}}}{R_{\mathrm{f}}}. \end{aligned} \tag{3}$$

If the injected current i_{HN} is controlled as

$$i_{\mathrm{HN}} = -\left(\frac{e_{\mathrm{A}}}{R_0} + C_0\frac{\mathrm{d}e_{\mathrm{A}}}{\mathrm{d}t}\right). \tag{4}$$

From (3), the ground fault current i_{f} and the faulty phase voltage u_{A} will be limited to zero simultaneously. Therefore, the SLG fault arc can be extinguished, and the distribution network returns to normal operation.

It is worth noticing that the current arc suppression method used in this paper has strong adaptability to low-resistance grounding faults. Compared with the voltage arc suppression method, which controls the faulty phase voltage of 10 kV bus to zero, the control target of the current arc suppression method is the compensation of the total ground leakage current. Therefore, as long as the total ground leakage current of the distribution network is compensated, the ground fault current can be effectively suppressed even in the case of a metallic ground fault, thereby reducing the damage to other electrical equipment caused by the large residual current of the ground fault.

3. CONTROL METHOD FOR FFE

3.1 Design for active disturbance rejection control

According to the mentioned above, the equivalent circuit of the distribution network with FFE can be drawn, as shown in Fig. 2. i_{R} and i_{C} are the currents flowing through leakage resistance R_0 and capacitance C_0, respectively.

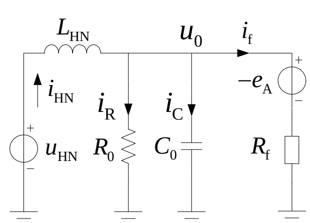

Fig. 2. The equivalent circuit of the distribution network with FFE.

From Fig. 2, the voltage across the filter inductor L_{HN} can be written as $u_{\mathrm{L}} = u_{\mathrm{HN}} - u_0$. Consequently, the injected current i_{HN} can be described by the differential equation as

$$\dot{i}_{\mathrm{HN}} = \frac{1}{L_{\mathrm{HN}}} u_{\mathrm{L}} = \frac{1}{L_{\mathrm{HN}}} u_{\mathrm{HN}} - \frac{1}{L_{\mathrm{HN}}} u_0. \tag{5}$$

According to Kirchhoff's current law (KCL), i_{C} can be expressed as

$$i_{\mathrm{C}} = C_0 \dot{u}_0 = i_{\mathrm{HN}} - i_{\mathrm{R}} - i_{\mathrm{f}} \tag{6}$$

Where the current flowing through the leakage resistance R_0 and fault resistance R_{f} can be expressed as $i_{\mathrm{R}} = u_0 / R_0$ and $i_{\mathrm{f}} = \left(u_0 + e_{\mathrm{A}}\right) / R_{\mathrm{f}}$, respectively. Therefore, the neutral-point voltage u_0 can be presented by the differential equation as

$$\dot{u}_0 = \frac{1}{C_0} i_{\mathrm{C}} = \frac{1}{C_0} i_{\mathrm{HN}} - \frac{1}{C_0}\left(\frac{1}{R_0} + \frac{1}{R_{\mathrm{f}}}\right) u_0 - \frac{1}{C_0 R_{\mathrm{f}}} e_{\mathrm{A}}. \tag{7}$$

The state-space representation [20] is written as

$$\begin{cases} \dot{\boldsymbol{x}} = \boldsymbol{A}\boldsymbol{x} + \boldsymbol{B}\boldsymbol{u} \\ \boldsymbol{y} = \boldsymbol{C}\boldsymbol{x} + \boldsymbol{D}\boldsymbol{u} \end{cases}. \tag{8}$$

From (5) and (7), the plant model can be rewritten as a state-space representation. Where the state variable $\boldsymbol{x}$, the input variable $\boldsymbol{u}$, and the output variable $\boldsymbol{y}$ can be described respectively as

$$\begin{aligned} \boldsymbol{x} &= \begin{bmatrix} x_1 & x_2 \end{bmatrix}^{\mathrm{T}} = \begin{bmatrix} i_{\mathrm{HN}} & u_0 \end{bmatrix}^{\mathrm{T}} \\ \boldsymbol{u} &= \begin{bmatrix} u_1 & u_2 \end{bmatrix}^{\mathrm{T}} = \begin{bmatrix} u_{\mathrm{HN}} & e_{\mathrm{A}} \end{bmatrix}^{\mathrm{T}} \\ \boldsymbol{y} &= \begin{bmatrix} i_{\mathrm{HN}} \end{bmatrix}. \end{aligned} \tag{9}$$

Moreover, the matrix can be derived as

$$\begin{gathered} \boldsymbol{A} = \begin{bmatrix} 0 & -\dfrac{1}{L_{\mathrm{HN}}} \\ \dfrac{1}{C_0} & -\dfrac{1}{C_0}\left(\dfrac{1}{R_0} + \dfrac{1}{R_{\mathrm{f}}}\right) \end{bmatrix}, \boldsymbol{B} = \begin{bmatrix} \dfrac{1}{L_{\mathrm{HN}}} & 0 \\ 0 & -\dfrac{1}{C_0 R_{\mathrm{f}}} \end{bmatrix}, \\ \boldsymbol{C} = \begin{bmatrix} 1 & 0 \end{bmatrix}, \boldsymbol{D} = \begin{bmatrix} 0 & 0 \end{bmatrix}. \end{gathered} \tag{10}$$

Let $\alpha = -1/L_{\mathrm{HN}}$, $\beta = 1/L_{\mathrm{HN}} = -\alpha$, $g = -\left(1/R_0 + 1/R_{\mathrm{f}}\right)/C_0$, $\gamma = 1/C_0$, $b = -1/\left(C_0 R_{\mathrm{f}}\right)$, the state-space representation of the plant model can be restated as

$$\begin{cases} \dot{x}_1 = \alpha x_2 + \beta u_1 \\ x_2 = \gamma x_1 + g x_2 + b u_2 \\ y = x_1 \end{cases}. \tag{11}$$

Because the fault resistance R_{f} is unknown and changes with time, the value of g and b are unknown. The certain intermediate value b_0 within the range of $b(t)$ is adopted, and let

$$f(x_1,x_2,t)=gu_0=-\frac{1}{C_0}\left(\frac{1}{R_0}+\frac{1}{R_\mathrm{f}}\right)u_0 \\ =f_0(x_1,x_2,t)+f_1(x_1,x_2,t) \\ =-\frac{1}{C_0R_0}u_0-\frac{1}{C_0R_\mathrm{f}}u_0. \tag{12}$$

Consequently, (11) can be represented as

$$\begin{cases}\dot{x}_1=\alpha x_2+\beta u_1\\ \dot{x}_2=\gamma x_1+f(x_1,x_2,t)+(b-b_0)u_2+b_0u_2\\ y=x_1\end{cases}. \tag{13}$$

Where the disturbance $f_0(x_1,x_2,t)=-u_0/(C_0R_0)$ is known and the disturbance $f_1(x_1,x_2,t)=-u_0/(C_0R_\mathrm{f})$ is unknown for the plant. If the insulation parameter measurement errors are considered, let $C_0=C_{0\mathrm{n}}+\Delta C_{0\mathrm{n}}$, $R_0=R_{0\mathrm{n}}+\Delta R_{0\mathrm{n}}$. Where C_0 and R_0 are the actual capacitance and resistance, respectively. $C_{0\mathrm{n}}$ and $R_{0\mathrm{n}}$ are the measured capacitance and resistance, respectively. $\Delta C_{0\mathrm{n}}$ and $\Delta R_{0\mathrm{n}}$ are the errors between the actual value and the measured value for capacitance and resistance, respectively. The disturbances are ubiquitous in the system due to the unknown fault resistance and insulation parameter measurement errors. In addition, the sampling errors from potential/current transformers can also be considered disturbances. Hence, the γ, g, and b contain unknown disturbance factors.

The schematic diagram of the first-order linear ADRC is shown in Fig. 3. It contains a linear state error feedback (LSEF) control, a linear extended state observer (LESO), and a disturbance compensation term (DCT). i_ref is the reference value of the injected current. i_HN is the measured value of the injected current. e_2 is the error between the feedback value i_HN and the estimated value z_1. e_1 is the error between the reference value i_ref and the estimated value z_1.

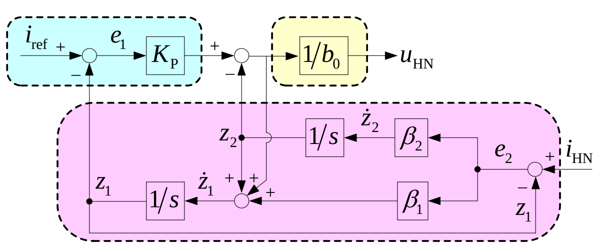

Fig. 3. Schematic diagram of first-order linear ADRC.

Design a linear expansion state observer (LESO) for first-order linear ADRC to reject the disturbances mentioned above, as follows

$$\begin{cases}\dot{z}_1=z_2-\beta_{01}(z_1-y)+bu\\ \dot{z}_2=-\beta_{02}(z_1-y)\end{cases}. \tag{14}$$

Where z_1 is the estimated value of the injected current i_{HN}, and z_2 is the estimated value of the disturbance. As shown in Fig. 3, the state variable can be observed via the output and input of LESO. When the e_2 approaches zero, the feedback i_{HN} can be tracked by z_1 of LESO, and $e_1 = i_{\mathrm{ref}} - z_1$ approaches to $i_{\mathrm{ref}} - i_{\mathrm{HN}}$. The disturbance of the plant can be estimated accurately by the observed value z_2. Therefore, the state variable and disturbance can be observed well by LESO, and the disturbance signal can be rejected.

3.2 Soft grid-connection scheme

At the initial time of the SLG fault, FFE tracks the voltage at the junction point in an open-loop manner. Then, the FFE starts to inject current into the distribution network. The two operation modes of FFE are different completely, so the injected current impulse may occur during the transient dynamics. Thus, the amplitude and phase of the voltage at the junction point (neutral point) should be changed regularly.

During FFE tracking the voltage at the junction point in an open-loop manner, the amplitude and phase of the output voltage u_{HN} are the same as that of neutral-point voltage u_0. Accordingly, the injected current i_{HN} is equal to zero according to Fig. 3. Later, the error $|e_{\mathrm{i}}|$ between the reference current and injected current is calculated to determine whether it is less than the threshold $e_{\mathrm{i}}^{\mathrm{th}}$. If not, FFE continues to track the neutral-point voltage until $|e_{\mathrm{i}}| > e_{\mathrm{i}}^{\mathrm{th}}$. Then, the amplitude and phase of the faulty phase to ground voltage and neutral-point voltage are calculated. In this way, the target trajectory based on the polynomial can be designed using steady-state constraints for the switching of the two operation modes. It can be designed as

$$\begin{cases} U_{\mathrm{ref}}^{\mathrm{amp}}(k+1) = U_0^{\mathrm{amp}}(k) + \left[E_{\mathrm{f}}^{\mathrm{amp}}(k) - U_0^{\mathrm{amp}}(k)\right]\dfrac{p(k)}{n} \\ \theta_{\mathrm{ref}}(k+1) = \theta_0(k) + \left[\theta_{\mathrm{f}}(k) - \theta_0(k)\right]\dfrac{p(k)}{n} \end{cases}. \tag{15}$$

Where $p(k) = k$, and $k = 1, 2, ..., n$. The neutral-point voltage amplitude U_0^{amp} is changed linearly to the amplitude of the faulty phase to ground voltage $E_{\mathrm{f}}^{\mathrm{amp}}$, and the neutral-point voltage phase θ_0 is changed linearly to the phase of faulty phase to ground voltage θ_{f}. The bistable smooth switching method can avoid the injected current impulse of FFE, and the FFE can realize a soft grid connection. The flow chart of the soft grid connection is shown in Fig. 4.

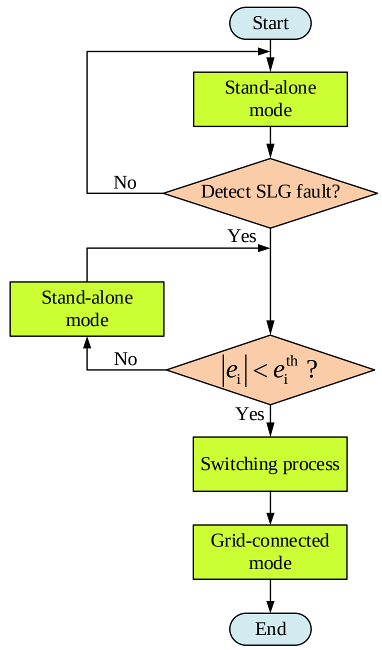

Fig. 4. Flow chart for soft grid connection.

4. SIMULATION AND DISCUSSION

4.1 Simulation parameters

A 10kV distribution network simulation model with an FFE was built according to Fig. 1. The damping rate in the distribution network is 8%. The FFE is a cascade H-bridge with 10 cascades, and the IDCM, the designed ADRC, and a soft grid-connection scheme based on bistable smooth switching are applied to it. The simulation step is set as 10 μs. The network specifications and control parameters in simulations are shown in Table I. The reference current error rate caused by the insulation parameter measurement errors and the sampling errors from potential/current transformers is 0.4%.

Table I Network specifications and control parameters in simulations.

Parameters	Value
Line-to-ground leakage resistance	5684 [Ω]
Line-to-ground capacitance	7 [μF]
Filter inductance	0.01 [H]
DC-link voltage of H-bridge cell	900 [V]
Switching frequency	10 [kHz]
ADRC β_1	100,000
ADRC β_2	1,000
ADRC $1/b$	10
ADRC K_P	250

4.2 Simulation results

The SLG fault occurs in phase A at $t = 0.025$ s. Fig. 5, Fig. 6, and Fig. 7 show the control performances of the PID, BSC, and ADRC with different fault resistances (10 Ω, 100 Ω, and 1000 Ω, respectively). The waveforms of injected current i_{HN}, SLG fault current i_{f} , and faulty phase voltage u_{A} are provided, and their transient dynamics at the moment of grid connection are highlighted. The soft grid connection using the zero-crossing detection method is adopted in the PID and BSC for comparison with using a bistable smooth switching scheme. In this way, the grid-connection time can be automatically identified.

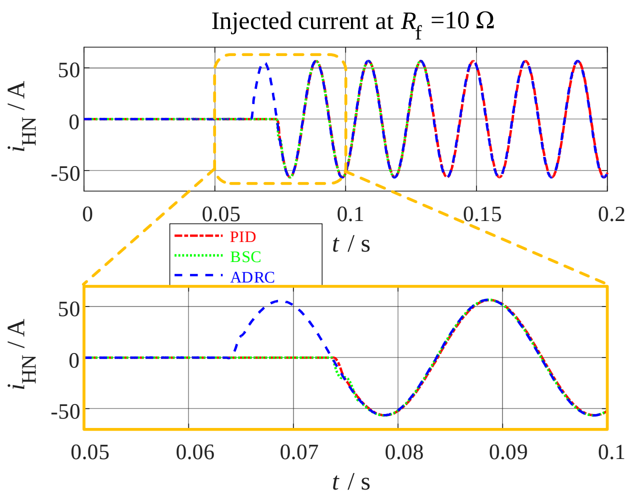

(a)

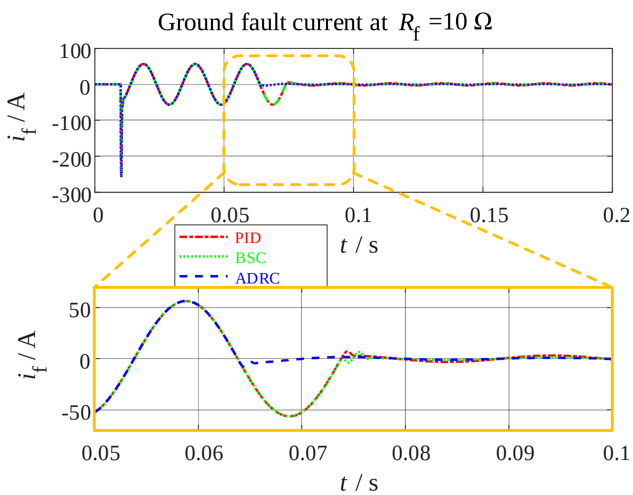

(b)

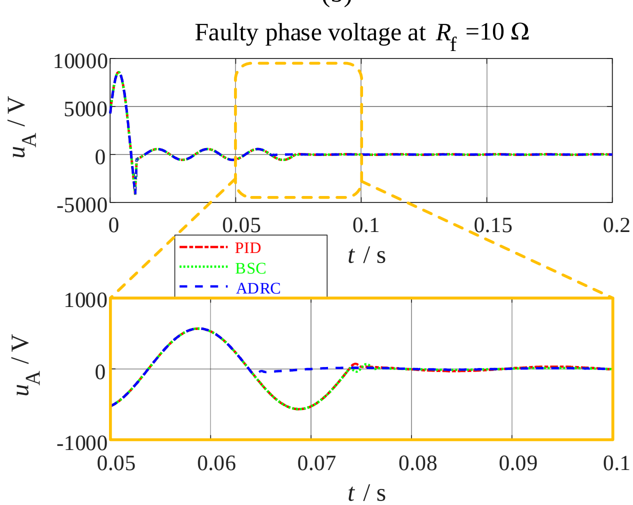

(c)

Fig. 5. Comparison between PID, BSC, and ADRC for 10 Ω SLG fault. (a) Waveforms of injected current; (b) Waveforms of ground fault current; (c) Waveforms of faulty phase voltage.

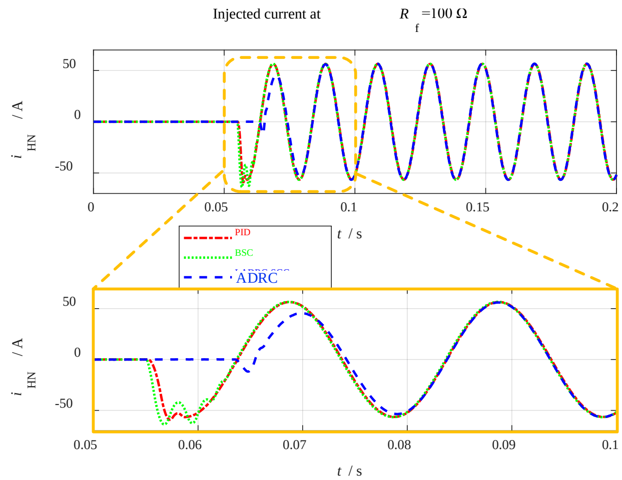

(a)

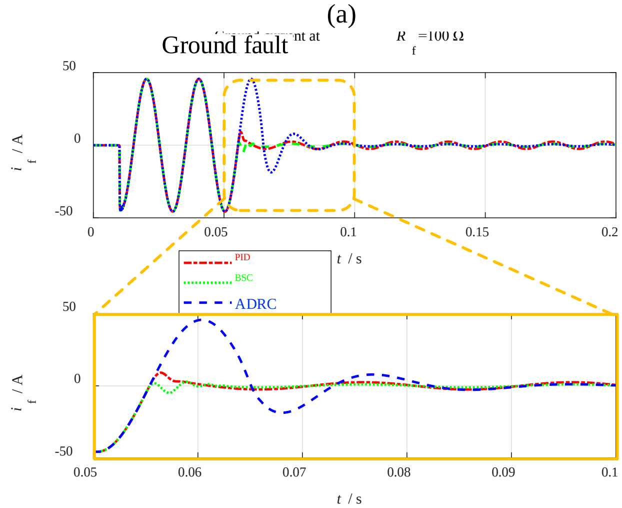

(b)

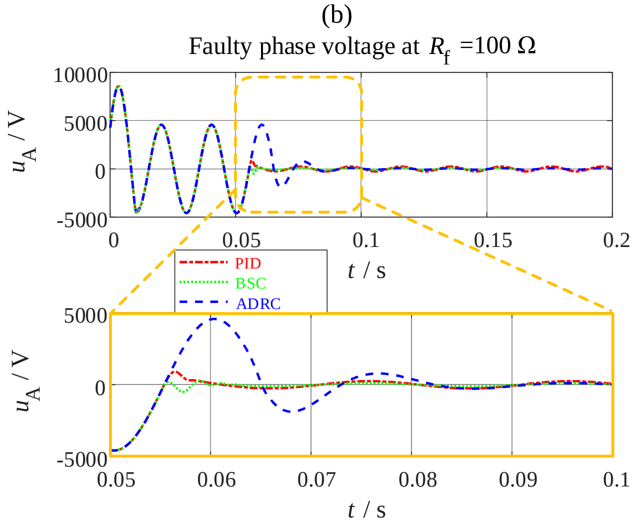

(c)

Fig. 6. Comparison between PID, BSC, and ADRC for 100 Ω SLG fault. (a) Waveforms of injected current; (b) Waveforms of ground fault current; (c) Waveforms of faulty phase voltage.

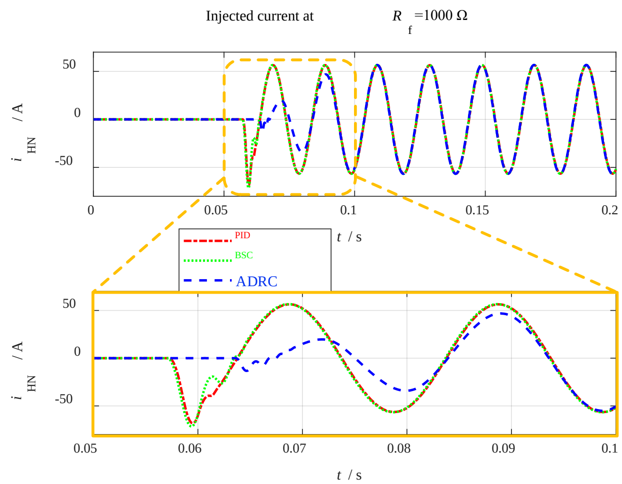

(a)

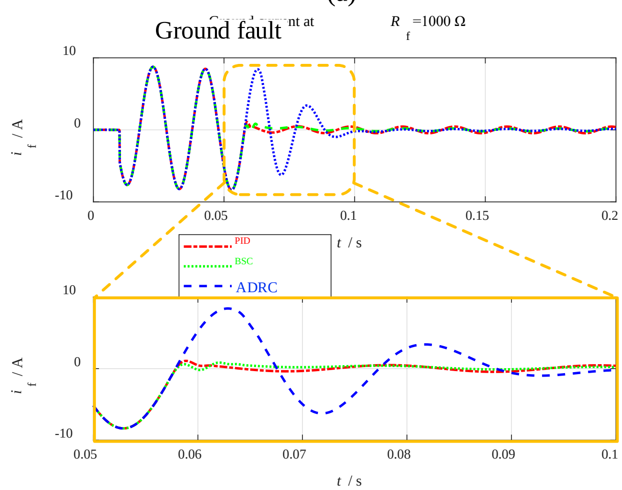

(b)

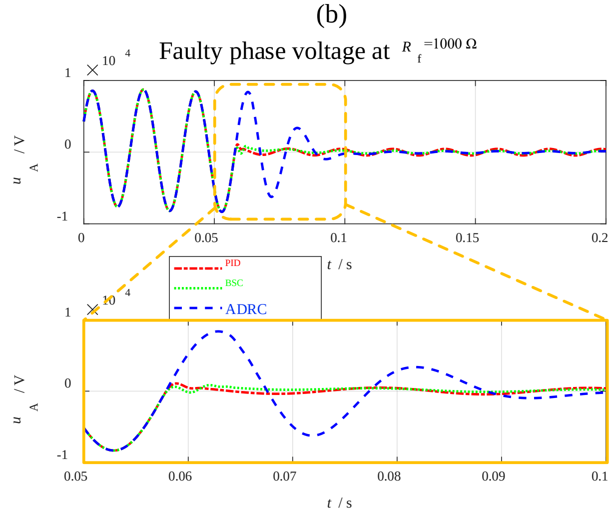

(c)

Fig. 7. Comparison between PID, BSC, and ADRC for 1000 Ω SLG fault. (a) Waveforms of injected current; (b) Waveforms of ground fault current; (c) Waveforms of faulty phase voltage.

Compared with the PID and BSC methods, the ADRC provides better performances in the case of variation of fault resistance. Because the insulation parameter measurement errors and the sampling errors from potential/current transformers can be properly corrected. Accordingly, the residual ground fault current based on the ADRC is minimal. Moreover, the grid-connection scheme based on bistable smooth switching can limit the injected current impulse well at the moment of grid connection in comparison to the zero-crossing detection method, which distinguishes its superiority with a large increase in fault resistance. Although the transient dynamics of soft grid connection may affect the speed of fault elimination, the FFE can start operation directly without waiting for the zero-crossing moment which may be delayed due to some factors such as harmonics. Therefore, according to the comprehensive evaluation, the proposed grid-connection scheme provides a faster response than the other methods.

Fig. 8 shows the residual ground fault current and residual faulty phase voltage controlled by the PID, BSC, and ADRC in the scenarios of different fault resistances. In this figure, the ADRC shows the best performance with the smallest residual ground fault current and faulty phase voltage. Hence, with the application of ADRC, the fault arc is of a great chance to get extinguished and the fault can be eliminated. The detailed simulation results of ADRC are shown in Table II. The root mean square (RMS) of the ground fault current is denoted as $I_{\mathrm{f}}^{\mathrm{RMS}}$, and the RMS of the residual ground fault current is defined as $I_{\mathrm{res}}^{\mathrm{RMS}}$. The rate of suppression of ground fault current is described as $\eta = \left(I_{\mathrm{f}}^{\mathrm{RMS}} - I_{\mathrm{res}}^{\mathrm{RMS}}\right) / I_{\mathrm{f}}^{\mathrm{RMS}} \times 100\%$.

Table II Simulation results.

$R_{\mathrm{f}}\,[\Omega]$	$I_{\mathrm{f}}^{\mathrm{RMS}}\,[\mathrm{A}]$	$I_{\mathrm{res}}^{\mathrm{RMS}}\,[\mathrm{A}]$	$\eta\,[\%]$
10	39.90	0.67	98.32
50	37.27	0.62	98.33
100	32.32	0.54	98.33
500	11.31	0.19	98.32
1000	5.90	0.10	98.33
5000	1.21	0.02	98.30
10000	0.61	0.01	98.25

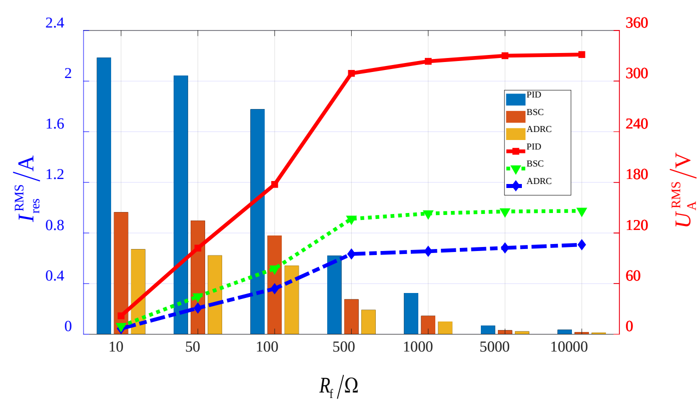

Fig. 8. Comparison of residual ground fault current (histogram) and faulty phase voltage (line chart) between PID, BSC, and ADRC under different SLG fault resistances.

Fig. 9 shows the injected current and zero-sequence voltage controlled by PID, BSC, and ADRC in the scenarios of different fault resistances. In comparison with the PID and BSC, the injected current based on ADRC is higher and closer to the actual value, thus, the reference current error caused by the insulation parameter measurement errors and the sampling errors from potential/current transformers can be properly corrected. And the zero-sequence voltage based on ADRC is more stable when the fault resistance varies. Thus, the disturbance impacts brought by the parameter measurement deviations and the sampling errors can be rejected.

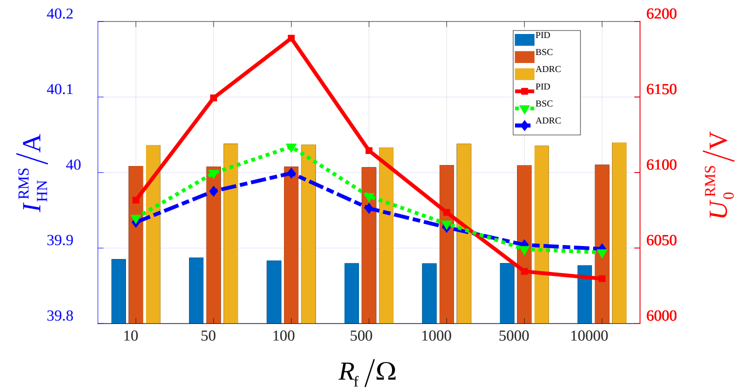

Fig. 9. Comparison of injected current (histogram) and zero-sequence voltage (line chart) between PID, BSC, and ADRC under different SLG fault resistances.

It is worth noticing that the generator current is almost not affected by the integration of the FFE into the distribution network. As shown in Fig. 2, the neutral point of distribution networks is not grounded. The connection between G and the 10 kV distribution network is isolated through a transformer $\mathrm{T_{yd}}$. Consequently, the zero-sequence current cannot flow into the high-voltage side of the transformer, i.e., the 110 kV power grid, and can only circulate on the low-voltage side, i.e., the 10 kV distribution network. Similarly, the zero-sequence current cannot flow into the low-voltage side of the distribution transformer, i.e., the 0.4 kV power grid, and can only circulate on the high-voltage side of the distribution transformer, i.e., the 10 kV distribution network. Thus, the load current is almost not influenced by the integration of the FFE into the distribution network.

5. EXPERIMENT AND DISCUSSION

5.1 Experimental parameters

As shown in Fig. 10, the SLG fault elimination is implemented by a prototype of the FFE on the 380V distribution network experimental platform. The prototype of FFE includes a CHB, a three-phase multi-winding isolation transformer for the DC power supply of H-bridge modules, a filter inductor, a contactor, and a three-phase adjustable transformer. The 380V distribution network experimental platform contains an SLG fault generator, and the detailed specifications of the platform are described in [6]. The network specifications and control parameters in this SLG fault elimination experiment are presented in Table III.

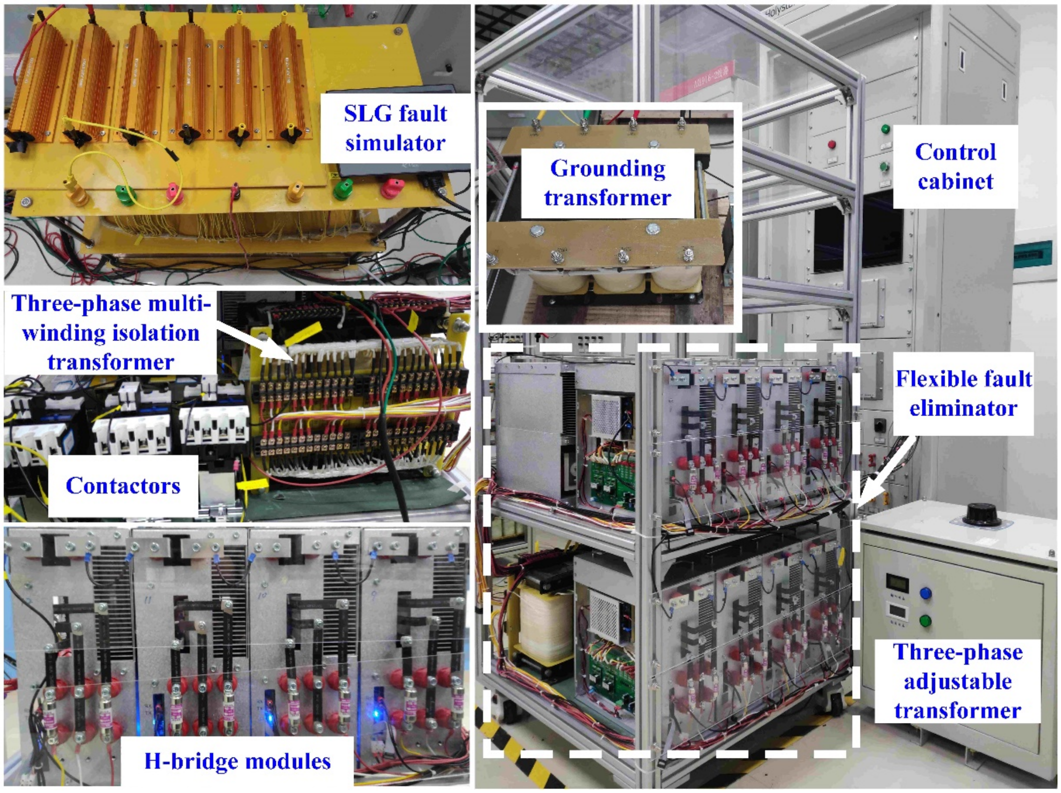

Fig. 10. Photograph of the prototype of FFE on the 380V distribution network experimental platform.

Table III Network specifications and control parameters in experiments.

Parameters	Value
Line-ground leakage resistance	800 [Ω]
Line-to-ground capacitance	12.893 [μF]
Number of H-bridge cells	12
Filter inductance	58.33 [mH]
DC-link voltage of H-bridge cell	50 [V]
Switching frequency	6 [kHz]
Control parameters of ADRC β_1	12,000
Control parameters of ADRC β_2	120
Control parameters of ADRC $1/b$	1.5
Control parameters of ADRC K_P	120

5.2 Experimental results

The SLG fault occurs in phase A. The performances of SLG fault elimination in the case of different ground fault resistance are shown in Fig. 11-Fig. 15. At the initial time, FFE tracks the voltage at the junction point in an open-loop manner. After the two gird cycles, the FFE starts to inject current into the distribution network. In these figures, u_{HN} is the output voltage of the FFE, and u_0 is the zero-sequence voltage of the distribution network, and i_f is the SLG fault current, and i_{HN} is the injected current of the FFE.

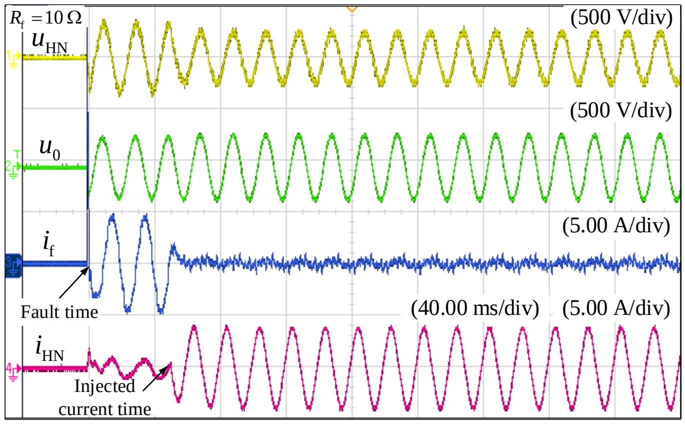

Fig. 11. SLG fault elimination in the case of 10 Ω fault resistance.

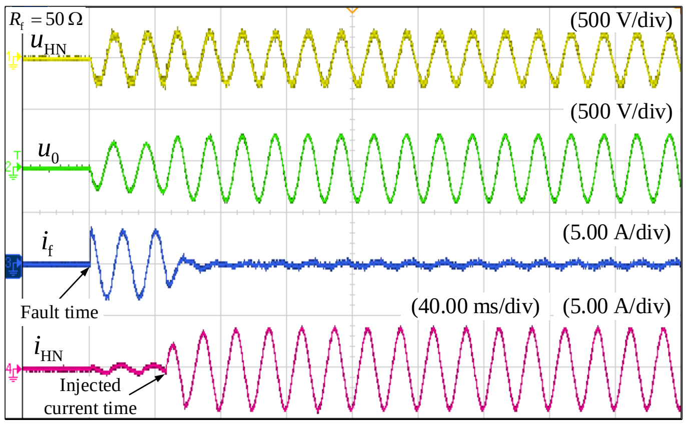

Fig. 12. SLG fault elimination in the case of 50 Ω fault resistance.

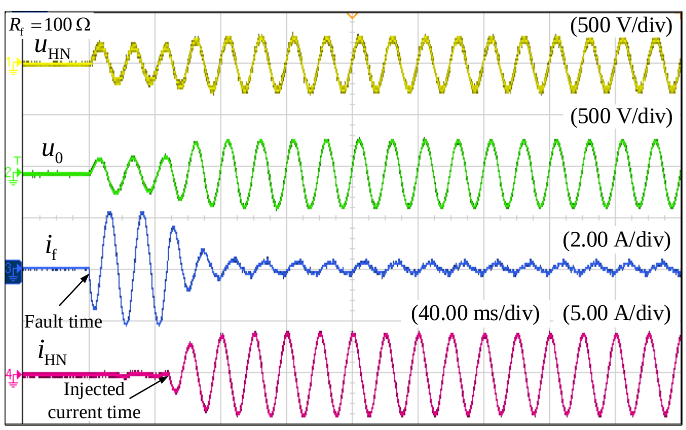

Fig. 13. SLG fault elimination in the case of 100 Ω fault resistance.

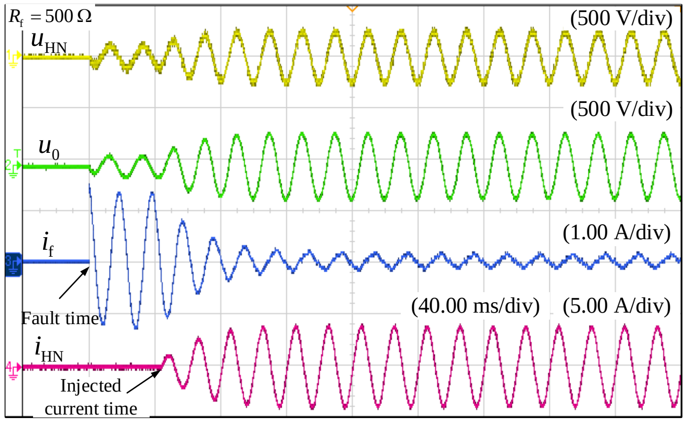

Fig. 14. SLG fault elimination in the case of 500 Ω fault resistance.

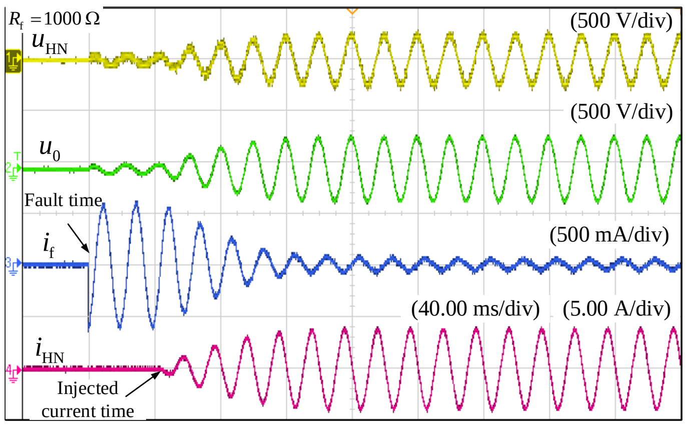

Fig. 15. SLG fault elimination in the case of 1000 Ω fault resistance.

The detailed experimental data are shown in Table IV. The ground fault current and faulty phase voltage are limited to small enough values to extinguish the fault arc in various ground fault conditions.

Table IV Experimental results.

R_f [Ω]	U_0^{RMS} [V]	U_f^{RMS} [V]	I_{res}^{RMS} [mA]	I_{HN}^{RMS} [A]
10	222.6	3.36	336.0	2.712
50	226.4	10.70	214.0	2.704
100	225.1	14.42	144.2	2.679
200	222.4	16.50	82.5	2.670
500	221.0	18.85	37.7	2.686
1000	219.1	18.95	18.95	2.677
2000	215.1	19.48	9.74	2.651
3000	215.0	21.21	7.07	2.652
5000	215.2	22.60	4.52	2.654
10000	215.0	28.40	2.84	2.654

According to the experimental results, the injected current i_{HN} increases smoothly from zero to the reference current value, proving that the soft grid-connection scheme based on bistable smooth switching can avoid the injected current impulse. The fault current i_f is limited as the injected current increases. Then, the injected current is adjusted continuously and slightly by the

ADRC, so the reference current error caused by the insulation parameter measurement errors and the sampling errors from potential/current transformers are properly corrected and the fault current is further limited to a lower value. Consequently, the FFE can flexibly and stably eliminate the SLG fault in the distribution networks with great robustness.

6. CONCLUSION

To avoid the hazards of the single-line-to-ground (SLG) fault and to ensure the safe and reliable operation of the distribution networks, this paper proposed a flexible fault eliminator (FFE) based on a cascaded H-bridge topology to limit the SLG fault current and extinguish fault arc in the medium voltage distribution networks. Moreover, an active disturbance rejection control (ADRC) for FFE was designed to correct the reference current errors caused by the insulation parameter measurement errors and the sampling errors from potential/current transformers. Furthermore, a soft grid-connection scheme based on bistable smooth switching was proposed to avoid the injected current impulse of FFE at the moment of grid connection. Simulation and experimental results showed that the ADRC with great robustness applies to different ground fault resistances. The output current and voltage of FFE at the time of grid connection were in a smooth transition, avoiding the impulse on the power grid system. With the increasing penetration rate of renewable energy, there are more disturbances in the distribution networks. The proposed method in this paper has enhanced resilience capabilities for realizing the reliable suppression of ground fault current, which will better adapt to future changes in the distribution networks.

7. ACKNOWLEDGMENTS

This work is supported in part by the National Natural Science Foundation of China under Award 51677030, and in part by the Natural Science Foundation of Fujian Province, China under Award 2023J05106. Furthermore, the authors express their sincere gratitude to the Referees and the Associate Editor for their thoroughness in reviewing this manuscript and their valuable advice.

8. REFERENCES

[1] Y. L. Liang, K. J. Li, Z. Ma, and W. J. Lee, "Typical Fault Cause Recognition of Single-Phase-to-Ground Fault for Overhead Lines in Nonsolidly Earthed Distribution Networks," IEEE Trans. Ind. Appl., vol. 56, no. 6, pp. 6298-6306, Nov.-Dec. 2020.

[2] A. Cerretti, F. M. Gatta, A. Geri, S. Lauria, M. Maccioni. and G. Valtorta, "Ground Fault Temporary Overvoltages in MV Networks: Evaluation and Experimental Tests," IEEE Trans. Power Deli., vol. 27, no. 3, pp. 1592-1600, July. 2012.

[3] Brenna M, De Berardinis E, Carpini L D , Paulon P, Petroni P, and Sapienza G, et al., "Petersen Coil Regulators Analysis Using a Real-Time Digital Simulator," IEEE Trans. Power Deli., vol. 26, no. 3, pp. 1479-1488, July. 2011.

[4] Rorabaugh J, Swisher A, Palma J, Andaya G, Webster M, and Kirkpatrick B, et al., "Resonant Grounded Isolation Transformers to Prevent Ignitions From Powerline Faults," IEEE Trans. Power Deli., vol. 36, no. 4, pp. 2287-2297, Aug. 2021.

[5] Colella P, Napoli R, Pons E, Tommasini R, Barresi A, and Cafaro G, et al., "Currents Distribution During a Fault in an MV Network: Methods and Measurements," IEEE Trans. Ind. Appl., vol. 52, no. 6, pp. 4585-4593, Nov.-Dec. 2016.

[6] Z. Y. Zheng, M. F. Guo, T. Jin, and J. H. Liu, "A novel method of insulation parameters measurement based on hybrid flexible arc suppression device in distribution networks", Int. J. Electr. Power Energy Syst., vol. 130, Sep. 2021, Art. no. 106982.

[7] A. M. Dan, Z. Czira, and D. Raisz, "Decreasing the harmonic content of the fault current during single-phase to ground faults in compensated network," 2009 IEEE Bucharest PowerTech, 2009, pp. 1-5.

[8] M. Janssen, S. Kraemer, R. Schmidt, and K. Winter, "Residual current compensation (RCC) for resonant grounded transmission systems using high performance voltage source inverter," 2003 IEEE PES Transmission and Distribution Conf. Exposition (IEEE Cat. No.03CH37495), 2003, pp. 574-578 vol.2.

[9] Z. Y. Zheng, M. F. Guo, N. C. Yang, and T. Jin, "Single-phase flexible arc suppression device based on BSC-SOGI-PLL method for distribution networks". Int. J. Electr. Power Energy Syst., vol. 121, Oct. 2020, Art. no. 106100.

[10] Z. Y. Zheng, M. F. Guo, N. C. Yang, and T. Jin, "Flexible arc-suppression method based on improved distributed commutations modulation for distribution networks". Int. J. Electr. Power Energy Syst., vol. 116, Mar. 2020, Art. no. 105580.

[11] B. Verma and P. K. Padhy, "Robust Fine Tuning of Optimal PID Controller With Guaranteed Robustness," IEEE Trans. Ind. Electron., vol. 67, no. 6, pp. 4911-4920, June. 2020.

[12] J. Wang and G. Yang, "Data-Driven Output-Feedback Fault-Tolerant Compensation Control for Digital PID Control Systems With Unknown Dynamics," IEEE Trans. Ind. Electron., vol. 63, no. 11, pp. 7029-7039, Nov. 2016.

[13] C. W. Tao, C. M. Wang, and C. W. Chang, "A Design of a DC–AC Inverter Using a Modified ZVS-PWM Auxiliary Commutation Pole and a DSP-Based PID-Like Fuzzy Control," IEEE Trans. Ind. Electron., vol. 63, no. 1, pp. 397-405, Jan. 2016.

[14] W. Qiu, M. Guo, G. Yang, and Z. Zheng, "Model-Predictive-Control-Based Flexible Arc-Suppression Method for Earth Fault in Distribution Networks," IEEE Access, vol. 7, pp. 16051-16065, Jan. 2019.

[15] Z. Y. Zheng, J. F. Xu, B. L. Zhang, H. Wang, M. F. Guo, and S. Y. Lin. "Flexible neutral point displacement overvoltage suppression method based on backstepping control in unbalanced distribution networks," Int. J. Electr. Power Energy Syst., vol. 148, Jun. 2023, Art. no. 108950.

[16] W. Tan and C. Fu, "Linear Active Disturbance-Rejection Control: Analysis and Tuning via IMC," IEEE Trans. Ind. Electron., vol. 63, no. 4, pp. 2350-2359, April. 2016.

[17] J. Han, "From PID to Active Disturbance Rejection Control," IEEE Trans. Ind. Electron., vol. 56, no. 3, pp. 900-906, March. 2009.

[18] Y. Su, X. Ge, D. Xie, and K. Wang, "An Active Disturbance Rejection Control-Based Voltage Control Strategy of Single-Phase Cascaded H-Bridge Rectifiers," IEEE Trans. Ind. Appl., vol. 56, no. 5, pp. 5182-5193, Sept.-Oct. 2020.

[19] Y. A. I. Mohamed, "Suppression of Low- and High-Frequency Instabilities and Grid-Induced Disturbances in Distributed Generation Inverters," IEEE Trans. Power Electron., vol. 26, no. 12, pp. 3790-3803, Dec. 2011.

[20] H. Xu, F. Nie, Z. Wang, S. Wang, and J. Hu, "Impedance Modeling and Stability Factor Assessment of Grid-connected Converters Based on Linear Active Disturbance Rejection Control," J. Mod. Power Syst. Clean Energy, vol. 9, no. 6, pp. 1327-1338, November 2021.

[21] R. Zhou, C. Fu, and W. Tan, "Implementation of Linear Controllers via Active Disturbance Rejection Control Structure," IEEE Trans. Ind. Electron., vol. 68, no. 7, pp. 6217-6226, July. 2021.

[22] J. Li, S. Bhattacharya and A. Q. Huang, "A New Nine-Level Active NPC (ANPC) Converter for Grid Connection of Large Wind Turbines for Distributed Generation," IEEE Transactions on Power Electronics, vol. 26, no. 3, pp. 961-972, March 2011.

[23] R. Xu, C. Zhang, Y. Xu, Z. Dong, and R. Zhang, "Multi-Objective Hierarchically-Coordinated Volt/Var Control for Active Distribution Networks With Droop-Controlled PV Inverters," IEEE Trans. Smart Grid, vol. 13, no. 2, pp. 998-1011, Mar. 2022.

[24] Q. Li, Y. Zhang, T. Ji, X. Lin, and Z. Cai, "Volt/Var Control for Power Grids With Connections of Large-Scale Wind Farms: A Review," IEEE Access, vol. 6, pp. 26675-26692, 2018.

[25] G. -S. Lee, D. -H. Kwon and S. -I. Moon, "DC Current and Voltage Droop Control Method of Hybrid HVDC Systems for an Offshore Wind Farm Connection to Enhance AC Voltage Stability," IEEE Transactions on Energy Conversion, vol. 36, no. 1, pp. 468-479, March 2021.

[26] M. G. Taul, X. Wang, P. Davari, and F. Blaabjerg, "An Overview of Assessment Methods for Synchronization Stability of Grid-Connected Converters Under Severe Symmetrical Grid Faults," IEEE Trans. Power Electron., vol. 34, no. 10, pp. 9655-9670, Oct. 2019.

[27] H. Nian, Y. Shen, H. Yang, and Y. Quan, "Flexible Grid Connection Technique of Voltage-Source Inverter Under Unbalanced Grid Conditions Based on Direct Power Control," IEEE Trans. Ind. Appl., vol. 51, no. 5, pp. 4041-4050, Sept.-Oct. 2015.

[28] Z. Y. Zheng, M. F. Guo, T. Jin, and J. H. Liu, "Hybrid flexible arc suppression device based on soft grid connection strategy for MV distribution systems" IET Gener. Transmiss. Distrib., vol. 15, no. 17, pp. 2499-2512, July. 2020.